# Non-Intrusive Estimation of Single-Port Thevenin Equivalents in AC Grids

Slobodan N. Vukosavic and Aleksandar M. Stankovic

*Abstract*— **This paper deals with the estimation of parameters of a Thevenin equivalent in an AC grid. We consider the practically relevant case of measurements coming from a grid-connected inverter. Our focus is on non-intrusive measurements, as we postulate and later experimentally observe transients that occur in normal operation as the primary source of information. We notice that even during quiet, after work hours there are typically enough variations in the grid to enable successful convergence of our procedure. For completeness, we also consider the artificial case of no external variations and show that injection of very small current perturbations suffices for convergence. Our procedure is based on real-time monitoring of the estimated determinant of the regression matrix. Regression matrix properties are also used to evaluate the integrity of the estimates and to initiate a brief sequence of perturbation in rare cases of the exceptionally restful grid. The estimation algorithm is simple enough to be implementable on standard industrial controllers, yet robust and reliable in terms of speed of convergence.**

*Index Terms*— **AC grid, Thevenin equivalent, voltage stability, measurement errors, robust least squares, parameter estimation**

## I. INTRODUCTION

The widespread use of power electronics to interconnect components in new electric energy systems has brought the promise of unprecedented flexibility and performance. Such inverter-based AC grids are emerging in utility systems, in microgrids, and on-vehicle platforms such as more-electric ships and aircraft. At the same time, this evolution has brought in several new problems in protection, control, and operation. Several of these problems require accurate knowledge of the quantities at the interface of components and subsystems, and the Thevenin circuit equivalent in particular.

Parameters of the Thevenin equivalent are of the foremost importance in all three levels of control typically present in modern inverters – at the level of a single inverter (phase-locked loop PLL tuning), at the plant level (interactions among several inverters) [1] and the energy system level (analogous to conventional power system stabilizers). For example, these parameters are critical ingredients for designing the inverter current regulator, especially for tuning anti-resonance aspects when the output LCL filter is present. Other uses of the same set of parameters include fast model-based protection, studies of harmonic propagation, detection of system-wide events [2], component condition monitoring and fault diagnosis, models for power system analysis and simulation.

Practical identification of Thevenin equivalents in many ways mirrors developments in the sensorless operation of AC drives [3]. Focusing on the dominant frequency range of the signals used in identification, there exist roughly three classes of methods – fundamental (possibly with low-frequency modulation), harmonics, and PWM. While the last two classes yield direct information about the Thevenin equivalent at the corresponding frequency, they are often used to make inferences about the equivalent at the fundamental frequency. Our method belongs to the first class and achieves parameter error of a few percent or lower. An example of simultaneous use of pairs of harmonics is [4], and the parameter errors are larger, but acceptable for the study's aim, which is the power loss allocation. The use of PWM ripple is still an active area in sensorless drives [5]; for our purposes, however, the presence of the output LCL filter at the point of coupling of the inverter with the rest of the network limits the reach of such signals and makes them impractical for Thevenin equivalent estimation.

Practical identification of Thevenin equivalents can be classified along several lines, including single [6] vs. multiport access [7], and intrusive (signal injection) [8, 9] vs. non-intrusive (background variation) observation [10]. A recent development that modifies the regression model and produces an estimate in finite time is presented in [11].

In this paper, we focus on the single (electrical) port case and the non-intrusive, real-time variant; other options do have their merits, and we outline some straightforward extensions of our method that are relevant for them. Specifically, we describe signal acquisition and filtering procedure that prevents signal components generated by disturbances, noise, and asymmetries at frequencies from the fundamental to PWM from affecting the regression matrix. As a consequence, our estimates of the Thevenin parameters predominantly depend on intrinsic variations of real and reactive power, resulting in extraordinary accuracy. In many cases, such as high-power interconnections, the injection of probing signals is challenging, so we are primarily interested in methods that use background variations for identification while achieving sub-1% accuracy. Our implementation involves inverters, not only because they are the dominant technology today, but for two additional reasons:

This work has been supported by NSF under grant ECCS-1710944, by CURENT Engineering Research Center of the National Science Foundation and the Department of Energy under NSF Award Number EEC-1041877, by ONR under grant N00014-16-1-3028, and also by the project F-143 of the Serbian Academy of Sciences and Arts.

S.N. Vukosavic is with the Department of Electrical Engineering, The University of Belgrade, Serbia and Serbian Academy of Sciences and Arts (e-mail: boban@etf.rs)

A. M. Stanković is with the Department of Electrical Engineering and Computer Science of Tufts University, Medford, MA, USA (e-mail: astankov@ece.tufts.edu).

This article has been accepted for publication in a future issue of this journal, but has not been fully edited. Content may change prior to final publication. Citation information: DOI 10.1109/TPWRD.2020.3026976, IEEE Transactions on Power Delivery



1. They allow us to explore existing AC networks that are accessible to us, and which in all tested cases provided sufficient excitation for our algorithms, and 2. They allow us to create artificial electrically quiet networks in which we can establish the size of minimal injections needed for our algorithm to work. While in today's networks inverters are not readily available in every node, the ongoing developments in renewable energy are certainly increasing their presence and availability. In cases when the information about the equivalent is needed in a node without an inverter, an estimate may be derived from electrically close nodes with such equipment, or an inverter could be connected temporarily.

The rest of the paper is organized as follows – in Section II we describe the required precision of parameter estimates, in Section III we outline the estimation model and in Section IV we describe our solution. Section V presents our experimental results, and in Section VI we describe the closed-loop operation in which we inject small excitation currents to achieve convergence of the estimation procedure. Our brief discussion and conclusions are given in Section VII.

## II. The Accuracy Required in Grid Estimation

The parameters of a Thevenin equivalent are key in many studies that involve system reduction so that particular components and their interactions can be studied in detail. The key issue here is not just the size of the unreduced model, but also its fidelity, as large interconnections often span continents. Thus a properly identified Thevenin equivalent not only makes the model size manageable but also potentially improves the model's predictive ability. Parameters of the Thevenin equivalent enter numerous control-oriented models, ranging from generalized Nyquist-type stability characterization in component tuning [12,13], to voltage stability [14] and even fast wave-type phenomena [15] in power systems. To make our presentation concrete, in this paper, we focus on Thevenin equivalent for inverter-connected sources and loads. It is, however, quite safe to assume that Thevenin equivalents will be of interest even in a distant future and regardless of the evolution of the converter technology, as they are key quantities that characterize the interactions between energy sources and loads that share the same power network. Our method requires modest amounts of data (voltages and currents at the point of connection). In terms of parameter accuracy, the equivalent estimate should be no worse than the data describing interconnected components, and probably slightly better, as it captures the evolving operating conditions of the energy grid. In later sections, we show that the accuracy of our method is often better than 1%, which is certainly in the range needed for useful predictions of stability and component interactions.

## III. The Equivalent Circuit Derivation

With ac grids gradually replacing the extensive copper-and-iron hardware by power electronic devices, a growing number of sources and loads are connected via electronic interfaces such as converters. An example of a grid-side converter which is often used in 0.4 kV grids is shown in Fig. 1. A digitally controlled three-phase PWM bridge generates the pulsed voltages with averages corresponding to the grid-frequency 3-phase ac voltages.

In most cases, the digital controller performs the real and reactive power injection control task through the subordinate current shaping. To suppress the PWM ripple from entering the grid, most grid-side power converters include an *LCL* filter, as shown in Fig. 1. For grid synchronization and component control, the voltages across the output terminal of the grid-side converter are measured and readily available within the controller. The same holds for the output currents injected into the mains. In some very low power grid-side inverters, the currents injected into the grid are not measured to save on the cost of current sensors. In such cases, the grid-injected currents are typically estimated by subtracting the *LCL*-capacitor currents (measured to stabilize an *LCL*-loaded current loop) from the DC-link derived inverter current.

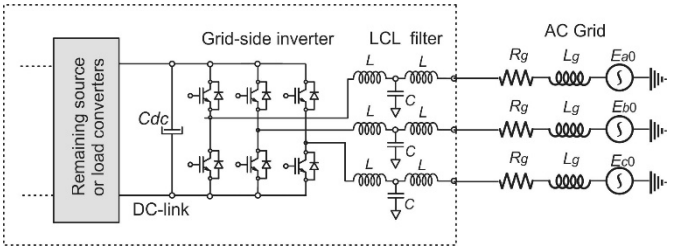


Fig. 1. A grid-side inverter connected to an ac grid.

The equivalent circuit of the grid-connected converter is given in Fig. 2. Electromotive forces $E_{a0}(t)$, $E_{b0}(t)$, and $E_{c0}(t)$ represent the open-circuit voltages of the ac grid at the connection point of the grid-side inverter. These voltages contain the line-frequency (fundamental) component, but in most cases, they also include several line-frequency harmonics. The currents $I_a(t)$, $I_b(t)$, and $I_c(t)$ are injected by the grid-side inverter (Fig. 1) into the ac grid. The inverter is equipped with a digital current controller which determines the PWM pulses and shapes the output current to obtain the desired active and reactive power. The voltages $U_{ia}$, $U_{ib,}$ and $U_{ic}$ of Fig. 2 are the voltages at the output of the grid-side converter; namely, at the point of the grid connection.

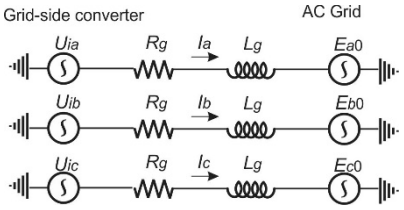


Fig. 2. Equivalent circuit with converter-generated voltages ($U_{ia}$, $U_{ib}$, $U_{ic}$), the grid equivalent impedance ($R_g$ and $L_g$), and with the grid no-load electromotive forces ($E_{a0}$, $E_{b0}$, $E_{c0}$).

Notice that the circuit of Fig. 2 possibly includes active or passive load connected to the grid. The subsequent developments and conclusions hold for such loads as well, provided that the voltages $U_i$ and terminal currents $I$ can be measured. After applying Clarke and Park transforms [16] on voltages $U$, $E$, and currents $I$, the circuit of Fig. 2 is described by

$$u_{id} = R_g i_d + L_g \frac{\mathrm{d}i_d}{\mathrm{d}t} - \omega_g L_g i_q + E_{0d}$$
$$u_{iq} = R_g i_q + L_g \frac{\mathrm{d}i_q}{\mathrm{d}t} + \omega_g L_g i_d + E_{0q} \quad , \qquad (1)$$

where $u_{id}$ and $u_{iq}$ represent the *dq*-frame components of the terminal voltages $U_i$, $i_d$, and $i_q$ represent the terminal currents $I$, $E_{0d}$, and $E_{0q}$ represent the grid open-circuit voltages $E_0$, while $\omega_g$ is the ac grid frequency expressed in (rad/s). In steady-state, the values $E_{0d}$ and $E_{0q}$ remain constant in cases when the open-circuit voltages are purely sinusoidal. Line frequency harmonics will contribute to oscillations of $E_{0d}$ and $E_{0q}$ components even in the steady-state.

In (1), $i_d$, $i_q$, $u_{id}$, and $u_{iq}$ are the terminal voltages and currents, which are measured and readily available within the controller of the grid-side converter. Parameters $R_g$ and $L_g$ define the Thevenin-equivalence impedance of the grid, and their estimation is the goal of the proposed solution. Values of $E_{0d}$ and $E_{0q}$ are assumed unknown and will be handled separately since they do affect the main estimation problem.

## IV. Proposed Methodology

Estimation of grid parameters $R_g$ and $L_g$ requires certain perturbation which could come out of the regular operation of the grid and grid-connected devices. In absence of native grid perturbation, it is possible to program the grid-side converter to inject the appropriate test signal. It is also possible to envision the operation where the perturbation intervals are followed by unperturbed steady-state intervals, provided that the parameters $R_g$ and $L_g$ do not exhibit significant variation during the latter intervals.

While the inverter switching in Fig. 1 introduces PWM perturbation into the grid, the amplitude of such perturbation is largely suppressed by the *LCL* filter. Moreover, estimation based on the PWM phenomena would yield the parameters $R_g$ and $L_g$ at the PWM frequencies which would be different due to the well-known frequency related variations.

Our objective is devising the estimation of grid parameters $R_g$ and $L_g$ without test signal injection and with no reference to PWM phenomena [13]. Instead, the intent is to rely on intrinsic fluctuations of the grid quantities as a readily available excitation and to provide the estimation method which provides reliable results even in cases where these fluctuations are very small. This would make the algorithm relevant for cases when the signal injection is not desirable or feasible, as in the high-voltage transmission grids. At the same time, the intent is to provide a practical, real-time assessment to allow tracking of possibly infrequent or intermittent network variations.

### *A. One-period averaging*

In principle, the estimation is based on correlating a relatively small voltage drop across $R_g$ and $L_g$ with corresponding currents. Thus, even a small error in $E_{0d}$ and $E_{0q}$, caused by line harmonics could impair the estimation procedure. To avoid the non-trivial task of estimating the line harmonics, it is possible to consider the average value of sampled voltages and currents within each line frequency period $T_g$. In (2), the average value of $u_{id}$ is calculated over the interval $[nT_g \,..\, (n+1)T_g]$. Similarly, one can obtain one-line-period average values $u^n_{iq}$, $i^n_d$, $i^n_q$, $E^n_{0d}$, and $E^n_{0q}$. With sufficient averaging, the values of $E^n_{0d}$ and $E^n_{0q}$ depend mostly on the fundamental voltage components and are not significantly affected by line-frequency harmonics. Any disturbance at frequencies that are multiples of $f_g = \omega_g/(2\pi) = 1/T_g$ does not change one-period average values.

$$u^n_{id} = \frac{1}{T_g} \int_{nT_g}^{(n+1)T_g} u_{id}(t)\,\mathrm{d}t \,. \qquad (2)$$

Applying one-line-period averaging (2) to voltage-balance equations (1), we obtain

$$u^n_{id} = R_g i^n_d + L_g \frac{\omega_g}{2\pi}\left[i_d\left(nT_g + T_g\right) - i_d\left(nT_g\right)\right] - \omega_g L_g i^n_q + E^n_{0d}$$
$$u^n_{iq} = R_g i^n_q + L_g \frac{\omega_g}{2\pi}\left[i_q\left(nT_g + T_g\right) - i_q\left(nT_g\right)\right] + \omega_g L_g i^n_d + E^n_{0q} \quad . \qquad (3)$$

In (3), the value $\Delta i^n_d := i_d(nT_g+T_g) - i_d(nT_g)$ represents the change of *d*-axis current on the interval $[nT_g \,..\, (n+1)T_g]$, calculated from the relevant samples of $i_d$ at the beginning and the end of the considered interval. The same holds for the value $\Delta i^n_q$. In practical application, the one-line-period average values are calculated by the grid-side converter digital controller from the samples of corresponding variables acquired on the considered interval. It is of interest to notice that the proposed calculations suppress the switching phenomena, and pass only the direct-sequence components of the voltages and currents while suppressing line harmonics, effects of asymmetries like the inverse-sequence component, disturbances, and noise. However, in the case of interharmonics that are very close to the fundamental, our simple averaging would likely have to be modified. While many filters could be candidates here, their effect on the accuracy and especially delay in estimates would have to be studied carefully.

### *B. Estimation of grid parameters*

It is reasonable to assume in practice that parameters $R_g$ and $L_g$ and the open-circuit line voltages $E^n_{0d}$ and $E^n_{0q}$ are constant over the intervals of $q$ successive $T_g$, with $q$ ranging from 10 to 100. The value of used in practice is network-dependent, and these values work well in cases that we encountered. With $E^n_{0d} = E_{0d} \,|\forall n$, and rewriting (3) for each of successive line periods from $n+1$ up to $n+q$, one obtains matrix equation (4), where the vector $U$ with $2q$ elements comprises the inverter voltages, rectangular matrix $A_{2q\times 4}$ comprises the line currents, while the vector $P_{4\times 1}$ comprises the unknown parameters.

The vector $P$ consists of four parameters that can be calculated using standard linear regression tools - by finding the Moore-Penrose pseudoinverse [18,19] of tall rectangular matrix $A$ (5). Provided that the considered data frame does not exceed a couple of hundreds of line-frequency periods, calculation of (5) can be performed in real-time, on typical digital signal controllers [20] used within electrical drives and grid-side converters.

This article has been accepted for publication in a future issue of this journal, but has not been fully edited. Content may change prior to final publication. Citation information: DOI 10.1109/TPWRD.2020.3026976, IEEE Transactions on Power Delivery



$$U=\begin{bmatrix} u_{id}^{n+1} \\ u_{iq}^{n+1} \\ u_{id}^{n+2} \\ u_{iq}^{n+2} \\ \cdots \\ u_{id}^{n+q} \\ u_{iq}^{n+q} \end{bmatrix} = \begin{bmatrix} i_d^{n+1} & \frac{\omega_g}{2\pi}\Delta i_d^{n+1}-\omega_g i_q^{n+1} & 1 & 0 \\ i_q^{n+1} & \frac{\omega_g}{2\pi}\Delta i_q^{n+1}+\omega_g i_d^{n+1} & 0 & 1 \\ i_d^{n+2} & \frac{\omega_g}{2\pi}\Delta i_d^{n+2}-\omega_g i_q^{n+2} & 1 & 0 \\ i_q^{n+2} & \frac{\omega_g}{2\pi}\Delta i_q^{n+1}+\omega_g i_d^{n+2} & 0 & 1 \\ \cdots & \cdots & \cdots & \cdots \\ i_d^{n+q} & \frac{\omega_g}{2\pi}\Delta i_d^{n+q}-\omega_g i_q^{n+q} & 1 & 0 \\ i_q^{n+q} & \frac{\omega_g}{2\pi}\Delta i_q^{n+q}+\omega_g i_d^{n+q} & 0 & 1 \end{bmatrix} \cdot \begin{bmatrix} R_g \\ L_g \\ E_{0d} \\ E_{0q} \end{bmatrix} = A \cdot P \tag{4}$$

$$P=\left(A^T \cdot A\right)^{-1} A^T \cdot U \,. \tag{5}$$

### C. Persistency of excitation and reliability of estimates

In cases where the system (1) is in steady-state, consecutive samples of *d-q* voltages and currents do not change much. In such conditions, det($A^TA$) is close to zero, and consequently, equation (5) cannot be used to estimate the parameters. In real-time applications, the *d-q* quantities are obtained from line voltages and currents that are sampled and converted within onboard analog-to-digital converters, processed through oversampling-related finite-impulse response (FIR) filters [21], and converter into the *d-q* frame by Clarke and Park transformations. Various manifestations of uncertainty, such as the ambient noise, imperfection of sensors, and quantization errors contribute to persistent change in all the signals. Thus, the situation where det($A^TA$) is equal to zero is hardly ever met, and expression (5) would yield the result even in the steady-state. In cases where intrinsic grid fluctuations provide sufficient excitation energy, expression (5) would yield reliable and credible estimates. However, in a steady-state, the result of (5) would also depend on intrinsic uncertainty, without any clear indication that the estimates are possibly incorrect. Thus, it is necessary to

i) Establish numerical means of getting an insight into the energy of the actual excitation signals in real-time,

ii) Use this insight in evaluating the reliability and credibility of the estimates.

It is well known [14,15] that the smallest singular value of $A$ captures the size of a perturbation $\Delta A$, where $\Delta A$ is the smallest matrix that reduces the rank of $\bar{A}=A+\Delta A$, and consequently make det($\bar{A}^T\bar{A}$)=0. Thus, the smallest singular value of $\sigma_{min}(A)$ is a measure of the excitation present in estimation. However, various system uncertainty and noise components also contribute to the observed $\sigma_{min}$. Thus, it seems hardly possible to derive an analytical expression for the threshold of $\sigma_{min}$ below which the estimates become unreliable. Instead, we rely to rely on experiments to compare the signal excitation energy, corresponding values of $\sigma_{min}$, and the estimation errors.

Although it is possible to calculate $\sigma_{min}$ in real-time, it would be a heavy burden for commonly used digital signal controllers [20] which typically provide 150-200 single-precision mega floating-point operations per second (MFLOPS). To avoid such a burden, it is possible to recall [18, 19] that the product of all the four singular values of $A$ equals the square root of det($A^TA$), the latter being calculated already as a side-result of (5). Thus, there is a monotonic relation between the real-time values of det($A^TA$), the amount of signal excitation energy brought in by the grid inherent fluctuations and the corresponding estimation error.

### D. Estimation in the presence of inconsistent excitation

The mechanism that supports an accurate estimation in the presence of volatile excitation is illustrated in Fig. 3. In cases where the excitation energy remains constant, $w_{eight}$ does not change, $G_{ain}$ remains constant, and the relation between the input $\hat{P}$ and the output $\tilde{P}$ of the circuit is defined by the first-order transfer function of (6), where the speed of convergence of the output towards the input is characterized by the time constant $1/G_{ain}$.

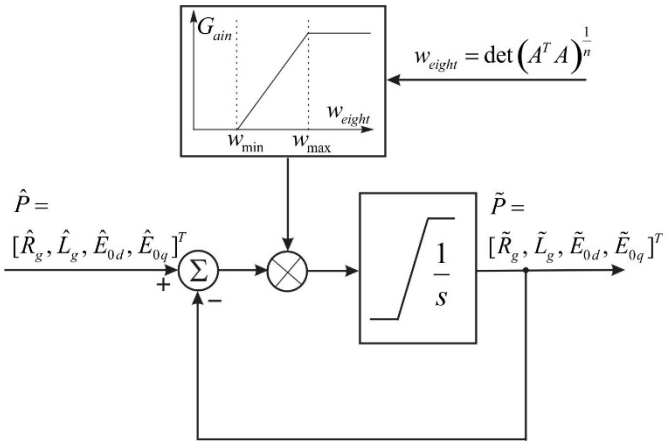


Fig. 3. The filter with variable gains where the convergence speed of the output towards the proposed input depends on approximated energy of excitation and, thus, on the reliability of the proposed input.

$$\tilde{P}=\frac{1}{1+\frac{s}{G_{ain}}}\hat{P}\cdot \tag{6}$$

The signal $w_{eight}$ in Fig. 3 rises with the energy of excitation. In cases where $w_{eight} < w_{min}$, $G_{ain}$ is equal to zero. In such cases, new estimates $\hat{P}$ do not have any impact on $\tilde{P}$, and the output retains the previous values. As the excitation energy and the signal $w_{eight}$ rise and the estimates $\hat{P}$ become more relevant, the output $\tilde{P}$ moves towards $\hat{P}$ more quickly. As the excitation grows, the value of $w_{eight}$ can assume very large values. Therefore, it is necessary to impose the limit to $G_{ain}$, to ensure that the dynamics of (6) remain decoupled from the principal time constants of the system. For the same reason, the signal $w_{eight}$ of Fig. 3 is obtained as the $n$-th root of det($A^TA$).

The structure of Fig. 3 has the potential of resolving the estimation problems in the presence of inconsistent excitation. Whenever the grid contains the inherent excitation of sufficient energy, the output in Fig. 3 will track the proposed estimates

while retaining the previously obtained (and still credible) values in all cases where the grid falls into near-steady-state conditions.

The thresholds $w_{min}$ and $w_{max}$ of Fig. 3 depend on the spectral content of the noise which, in turn, includes the noise that originates from the grid, the switching noise of static power converters, the noise of sensing devices, and analog prefiltering, as well as the quantization noise of analog to digital (A/D) acquisition and oversampling chain. Therefore, the best way to set the relevant thresholds and gains is to consider experimental data taken on a sample grid-side converter.

## V. Experimental Assessment of Requisite Excitation

For a proper tuning of the relevant thresholds and settings, it is necessary to check the minimum levels of the intrinsic, grid-induced excitation which are sufficient to obtain reliable estimates. The following set of tests sweeps through the relevant ranges of excitation frequencies and excitation amplitudes to establish the relationship between the excitation energy, corresponding singular values, $w_{eight}$ values, and the resulting estimation errors.

### *A. Experimental setup*

The relevant experiments were obtained on a laboratory setup with a grid-side inverter connected to 0.4 kV, 50 Hz AC grid. A simplified electrical schematic of the setup is shown in Fig. 4, while the disposition of the main components is shown in Fig. 5. The 3-level, 3-phase PWM converter is an IGBT-based T-type, neutral-point clamped NPC inverter which can run either in 2-level or 3-level mode. Since the modulation technique did not demonstrate any significant impact on the results, the experiments proceeded in the 2-level mode. The relevant voltage and current sensors are shown in Fig. 4. For the given setup, the values of the grid parameters are $L_g$= 207 μH and $R_g$= 98 mΩ.

Grid-side inverters include an *LCL* output filter to suppress the injection of PWM ripples into the grid with a reasonably-sized filter. To achieve stable operation of the digital current controller in the presence of an *LCL* load, the capacitor currents are measured in addition to the inverter output currents. In the absence of electromagnetic interference (EMI) components in Fig. 4, the sum of inverter currents is equal to zero. Therefore, only two inverter currents have to be measured. The third one can be reconstructed at the cost of being affected by the offsets and errors from both current sensors. The same considerations hold for the capacitor currents. The currents injected into the grid are denoted by $I_a$, $I_b$, and $I_c$ in Figs. 2 and 4. If the measurement errors and delays are negligible, the grid currents can be reconstructed from the available measurements according to relations $I_a = I_{iA} - I_{cA}$, $I_b = I_{iB} - I_{cB}$, and $I_c = -I_b - I_a$. Since it is necessary to measure the inverter currents with sensors capable of measuring both AC and DC components, the sensors used for capacitor currents could be plain AC sensors. However, the two sets of sensors would then rely on different technology and have different delays and measurement errors. In large-power inverters, an additional problem comes from the EMI filters used to meet stringent norms. These filters contribute to a high-frequency non-zero-sum of the three currents, which, in turn, excludes the possibility of relying on $I_c = -I_b - I_a$ and reducing the count of current sensors. In field applications, it is thus recommended to measure all grid currents by dedicated AC sensors. In most grid-side inverters with larger power ratings, reliability and performance aspects (such as the reactive power injection control) prevail over the cost concerns, and the grid-injected currents $I_a$, $I_b$, and $I_c$ are measured through dedicated ac sensors. The line voltages $U_{iAB}$ and $U_{iBC}$ are also measured (Fig. 4), as they are required for synchronization and control of the grid-side inverter.

The inverter operates with dc-bus voltages of $E_{DC}$ = 590 V, switching frequency of $f_{PWM}$ = 5 kHz, the lockout time of 3 μs, the rated current of 16 A, and the peak current of 50 A. During the tests, the grid-side resistance was deliberately changed by inserting precision small-resistance power resistors.

Control and signal processing tasks are performed by a floating-point digital signal processor with a 12-bit, 16-channel, direct memory access DMA-driven analog to digital conversion (ADC), particularly suited for the tasks of oversampling and FIR post-filtering which suppresses any PWM-related noise from the relevant measurements. The DMA/ADC units are programmed to (over)sample each channel at 160 kHz [2]. The control structure includes the DC-bus voltage controller. Notice in Fig. 4 that the DC-bus circuit does not have any external connection, so no average net power can be exchanged. Since the average power injected into the DC-bus circuit remains zero, the setup cannot perform any long-term injection of active power into the grid. On the other hand, reactive power injection is limited only by the rated and peak currents of the setup. In the case of significant and persistent frequency variations, the settings of the PLL can influence the operation of the parameter estimation algorithm, especially if the PLL bandwidth is high; we found that more modest settings advocated by industry tend to work well [23].

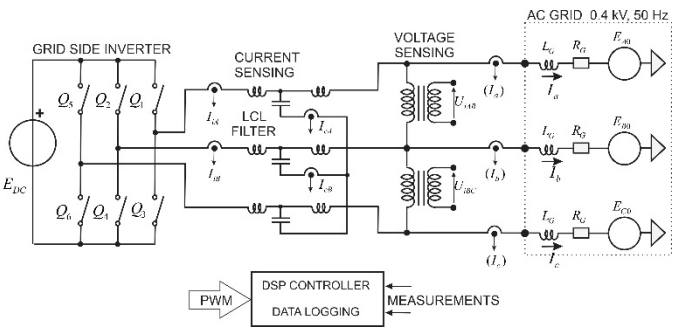


Fig. 4. Block diagram of the experimental setup. The grid-side inverter with an output LCL filter is connected to 0.4 kV 50 Hz ac grid. The Figure shows the relevant voltage and current measurements. The laboratory prototype of the grid-side inverter can run in both 2-level or 3-level modes. All measurements are taken in the 2-level mode.

Control and signal-processing software includes the most common grid-side inverter features with the option to inject desired active and reactive powers. Oversampled and FIR-filtered voltages and currents are firstly averaged over each PWM period, and then averaged over the grid-frequency periods (2) to obtain the elements of matrices and vectors of (4), later used in (5) to obtain and validate (Fig. 3) the estimates; relevant algorithms are mostly from [22]. The Digital current controller operates in the dq-frame. The closed-loop bandwidth

This article has been accepted for publication in a future issue of this journal, but has not been fully edited. Content may change prior to final publication. Citation information: DOI 10.1109/TPWRD.2020.3026976, IEEE Transactions on Power Delivery



and disturbance-rejection capability of the current controller provide the means for maintaining d- and q-axis currents at their set values even when the grid experiences considerable variation and/or distortion. By maintaining $I_d$ and $I_q$ at constant values, the setup can keep the matrix $A$ of (4) free of perturbations other than quantization errors and noise.

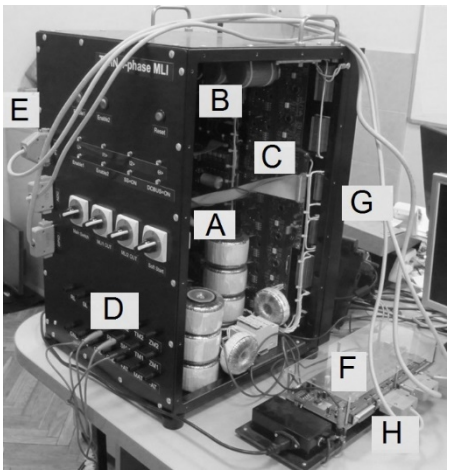


Fig. 5. Laboratory setup: (A) Output chokes of the *LCL* filter. (B) DC-bus components. (C) Bidirectional switches for the neutral-point clamping. (D) Grid connections. (E) Converter-side connections for PWM signals and analog measurements. (F) DSP controller with a real-time USB link. (G) Heatsink. (H) DSP-side connections for PWM and analog signals.

### *B. Steady-state with small oscillations of reactive power*

To obtain an insight into the smallest perturbation level which still yields reliable estimates, the experimental setup is programmed to run in steady-state, with rated reactive power and just a small superimposed sinusoidal variation of reactive current which ranges from 0.3 % up to 3 % of the converter rated current (that is, from 62 mA up to 500 mA). To explore the impact of the excitation frequency, the frequency of these variations is changed from 0.1 Hz up to 70 Hz. The size of matrix $A$ of (4) is set to cover 100 successive periods of line voltages. The relevant outcomes of each measurement include the estimates $R_g$ and $L_g$, the value of det($A^TA$), and the off-line calculated the smallest singular value of matrix $A$.

The results presented in Fig. 7 show that the proposed method provides $L_g$ estimates with a precision better than 1% even with excitations as low as 62 mA, provided that the excitation frequency remains between 0.3 Hz and 5 Hz. Notice that, whatever the excitation amplitude, the estimation errors increase when the frequency rises above 5 Hz. This result was expected, as the proposed method involves a great deal of filtering/averaging and focuses on background perturbation energy that originates from low-frequency fluctuations. Corresponding results of Fig. 6 prove that the relative estimation errors are larger for the parameter $R_g$. With the amplitude of 62 mA and with the frequencies ranging from 0.5 Hz up to 5 Hz, the $R_g$ errors remain below 3.2 %. To reduce the errors below 1 %, it is necessary to increase the excitation amplitudes up to 125 mA, and even 250 mA to achieve good performance in the whole range from 0.5 Hz to 20 Hz.

Corresponding values of the smallest singular value and det($A^TA$) are given in Figs. 8 and 9. The plots are made with logarithmic scaling on both axes. By comparing the results in the four plots, we conclude that the practical estimation of both $R_g$ and $L_g$ requires the smallest singular value not lower than 0.2, or, the value of det($A^TA$) not lower than 6000.

### *C. The setting of parameters $w_{min}$, $w_{max}$, and n.*

By setting the desired accuracy of $R_g$ and $L_g$ estimation to 1%, the obtained results in Figs. 6-9 and the subsequent considerations show that the point ($w_{min}$, $G_{ain}$= 0) in Fig. 3 should match det($A^TA$) ≈ 300. At the same, with excitations where det($A^TA$) > 30000, the estimates are reliable in a wide frequency range, and the gain $G_{ain}$ of Fig. 3 could be set to the maximum. In Figs. 6-9, variations of the excitation amplitude and the estimations errors of 1:10 go along with the change in det($A^TA$) of 1:1000. To obtain a relation between the excitation amplitudes, consequential errors, and det($A^TA$)$^{1/n}$, it is convenient to set $n$ = 3 or $n$ = 4. With $n$ = 3, we obtain $w_{min}$= 7 and $w_{max}$= 31. The maximum gain $G_{max}$ determines the smallest time constant 1/$G_{max}$, which should remain in the range of $q \cdot T_g$.

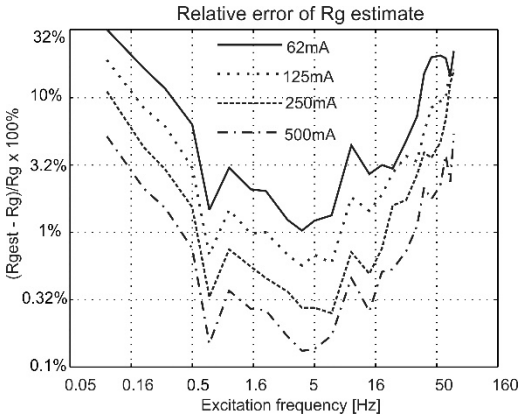


Fig. 6. The change in the relative error of $R_g$ estimation with the amplitude and frequency of superimposed reactive power.

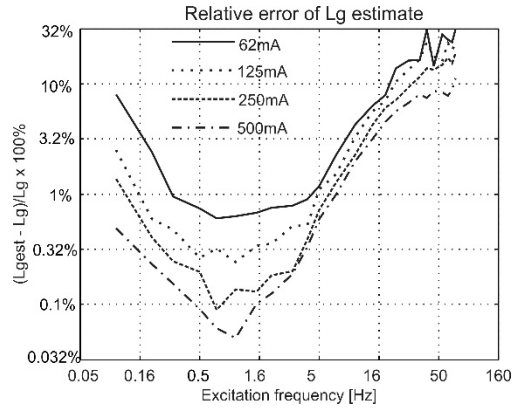


Fig. 7. The change in the relative error of $L_g$ estimation with the amplitude and frequency of superimposed reactive power.

This article has been accepted for publication in a future issue of this journal, but has not been fully edited. Content may change prior to final publication. Citation information: DOI 10.1109/TPWRD.2020.3026976, IEEE Transactions on Power Delivery



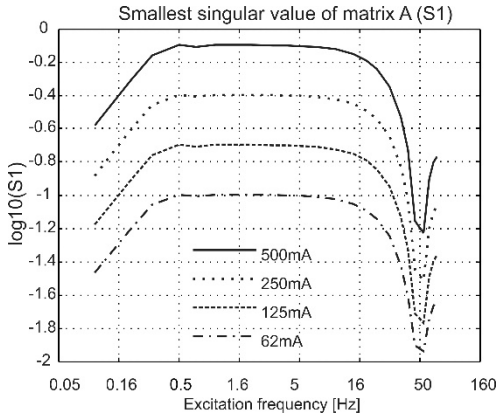


Fig. 8. The change in the smallest singular value with the amplitude and frequency of superimposed reactive power.

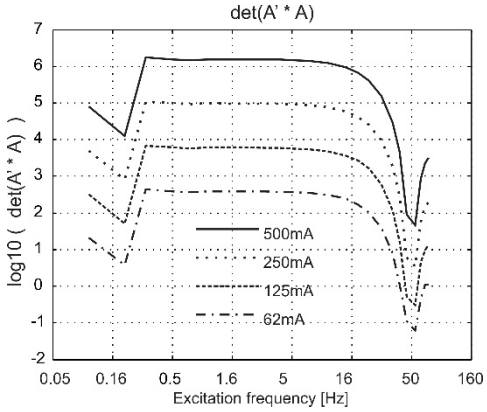


Fig. 9. The change in det($A^TA$) with the amplitude and frequency of superimposed reactive power.

### *D. Case study - intrinsic excitation in a typical 0.4 kV grid*

The proposed method relies on intrinsic fluctuations within the grid and depends on the excitation energy brought by such fluctuations. The experimental evidence (Figs. 6-9) proves that the accuracy of $R_g$ and $L_g$ estimation better than 1% requires the values of $\log_{10}[\det(A^TA)]$ which, depending on the excitation frequency, vary between 2.7 and 3.80. To get a preliminary insight into the excitation energy of a typical 0.4 kV AC grid, the line currents, and voltages are measured at the main switch box for a group of offices and laboratories during off-hours, picking a couple of minutes with the least load changes.

The collected data were processed to obtain $i_d$ and $i_q$ samples, the values that make part of the matrix $A$ of (4). The sample waveforms of Fig. 10 display the excitation energy which remains well above 3.8, even though the currents are close to steady-state. While there is no way to demonstrate that the excitation energy in all AC grids is going to be comparable to the one shown in Figs. 10 and 11, it is reasonable to expect occasional slow oscillations of either active or reactive current component in 0.4 kV grids with an amplitude of 125 mA or larger (Figs. 6-9). In Fig. 12 we display the largest and the smallest singular value of the matrix $A$ as functions of acquisition time.

## VI. CLOSED-LOOP OPERATION

It is of particular interest to verify the operation of the mechanism of Fig. 3 in cases where the excitation is intermittent, wherein the excitation-rich intervals are followed by prolonged intervals with insufficient energy of relevant signals. In such cases, the output $\tilde{P}$ of Fig. 3 moves towards the intermediate result $\hat{P}$ at a variable rate. The intermediate result $\hat{P}$ is obtained from (5), and its integrity depends on the excitation energy which is present within the system. The convergence rate is controlled by $w_{eight}$, a measure of the excitation energy obtained as the third root of det($A^TA$). With the proposed setting ($w_{min}$= 7, $w_{max}$= 31), the values of $\log_{10}(\det(A^TA))$ have to be lower than 2.5 to keep the mechanism of Fig. 3 in steady-state due to the lack of excitation. With larger values, it is not possible to test the modes where the mechanism of Fig. 3 crosses the threshold $w_{min}$. The available grid includes the excitation energy (Fig. 11) which cannot be reduced below $w_{min}$.

To test the circuit of Fig. 3 with very low excitation energies, it was necessary to use the digital current controller of a grid-side inverter (Figs. 4-5) without its outer loops that control active and reactive power. In this way, the values of $i_d$ and $i_q$ can remain unaffected by fluctuations of the grid, and the excitation introduced in (4) can be driven below $w_{min}$.

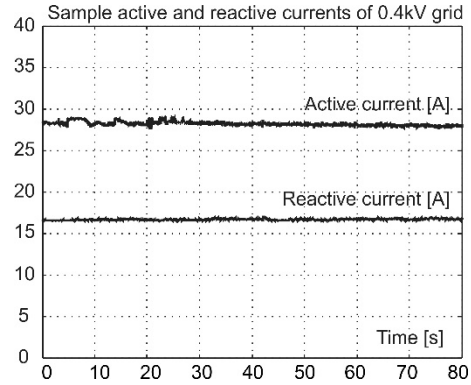


Fig. 10. Active and reactive current ($i_d$ and $i_q$) obtained from the voltage and currents measurements taken at the main switch box for a group of offices and laboratories during off-hours, the time interval with the least load changes.

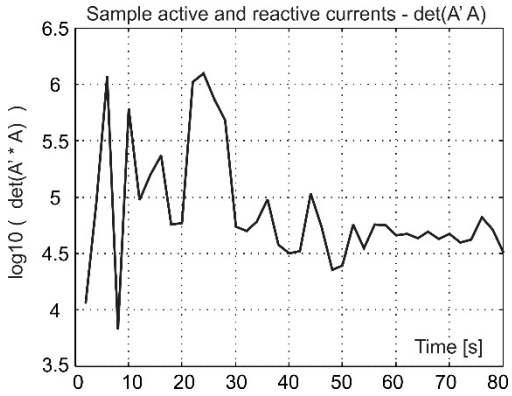


Fig. 11. Excitation comprised within active and reactive currents of Fig. 10, expressed in terms of $\log_{10}(\det(A^TA))$.

This article has been accepted for publication in a future issue of this journal, but has not been fully edited. Content may change prior to final publication. Citation information: DOI 10.1109/TPWRD.2020.3026976, IEEE Transactions on Power Delivery



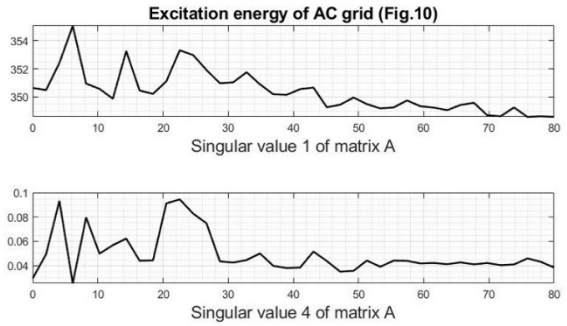


Fig. 12. The largest and the smallest singular values of matrix $A$ obtained with active and reactive currents of Fig. 10.

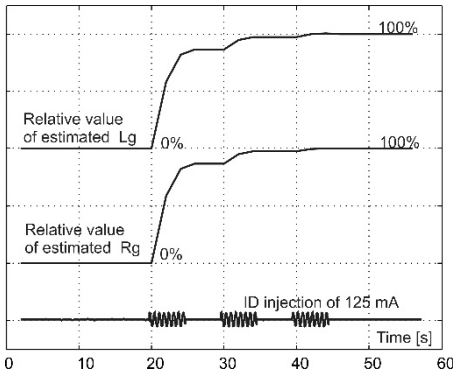


Fig. 13. Relative values of $R_g$ and $L_g$ estimates obtained by applying the structure of Fig. 3 with grid side inverter operated in the near-to-steady-state condition where only the current reference $i_d$ exhibits periodic oscillations with an amplitude of 125 mA.

To obtain the traces shown in Fig. 13, the grid-side inverter is brought into steady-state, where both $d$-axis and $q$-axis currents are kept constant, except for periodic, 5-seconds long bursts of low-frequency oscillations of $d$-axis current. The amplitude of oscillations is set to 125 mA. The plot in Fig. 13 shows the relative values of $R_g$ and $L_g$ estimates. The initial value of estimates is set to the (erroneous) value of zero. Whenever the $d$-axis disturbance increases the excitation energy above $w_{min}$ threshold, the estimation error decreases, and the estimates come closer to actual values of $R_g$ and $L_g$. Eventually, after the third burst, the relative values of both estimates come close to one per unit.

We also present performance results for the case of a sudden change in Thevenin parameters, say due to network switching. The line series resistance is increased by inserting a non-inductive series resistance roughly equal to 77% of the previous $R_g$ value. The test is performed with $d$-axis current excitation equal to 400mA. The waveforms in Fig. 14 represent the relative values of $R_g$ and $L_g$ estimates. Both estimates remain close to the actual grid parameters both before and after the operation of the switch. During the transient, $L_g$ estimate exhibits a relatively large deviation; the transient settles in roughly 7 seconds. It is also of interest to study the values of estimated open-circuit electromotive forces during the test shown in Fig. 14. The experimental waveform of the estimate of open-circuit voltage $E_q$ is given in Fig. 15 (the component $E_d$ behaves similarly, but its magnitude is less than 0.4V). The estimates of $E_d$, $E_q$ exhibit a delay that is slightly shorter than in the case of estimating the Thevenin impedance.

The impact of interharmonics on the proposed method is verified by computer simulation. Experimental verification was not feasible since the interharmonic content of the available ac grid remained below the quantization level of the analog signal acquisition chain. The simulations do not take into account quantization effects the A/D signal acquisition delays of the current controller and imperfections of the PWM. The amplitude of superimposed interharmonic is set to 1% with a frequency of 166 Hz. Corresponding waveforms are given in Fig. 6. The mean relative value of the $R_g$ parameter is 0.9907, thus, there is an error of 1%, which demonstrates that interharmonics do have an impact on the estimation. The mean relative value of the $L_g$ parameter is 0.9994, so the error caused by interharmonics is lower, but there is a noticeable variance.

## VII. Discussion and Conclusions

We proposed, implemented, and experimentally verified an algorithm that enables estimation of the R-L Thevenin equivalent in an AC network that achieves accuracy below 1% based only on background variations in voltage, real and reactive power that are present a majority of networks, without test signal injection. We practically verified our procedure in an AC grid supplying a small office building during off-hours. We think that this is encouraging, as many other AC grids would likely offer larger background excitation. For completeness, we also devise a closed-loop low-current injection scheme that works in cases of extremely quiet networks without causing adverse effects on typical loads.

Our procedure is based on real-time monitoring of the estimated determinant of the regression matrix which guards against poor numerical conditioning of parameter estimates. We demonstrate that the estimation algorithm is simple enough to be implementable on standard industrial controllers while being robust and reliable in terms of speed and quality of convergence.

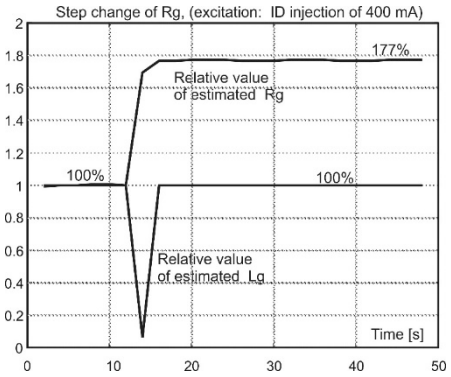


Fig. 14. Relative values of $R_g$ and $L_g$ estimates obtained with the setup of Fig. 4. The current reference $i_d$ exhibits periodic oscillations with an amplitude of 400 mA. After approximately 14 seconds, additional non-inductive resistance is inserted to increase $R_g$ by, roughly, 77%.

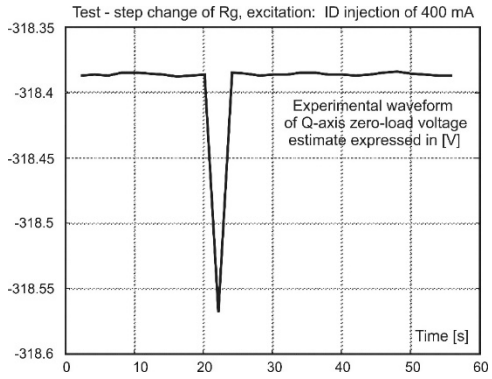


Fig. 15. Estimated open-circuit voltage in the *Q*-axis, obtained with the setup of Fig. 4. After approximately 22 seconds, additional non-inductive resistance is inserted to increase $R_g$ by, roughly, 77%.

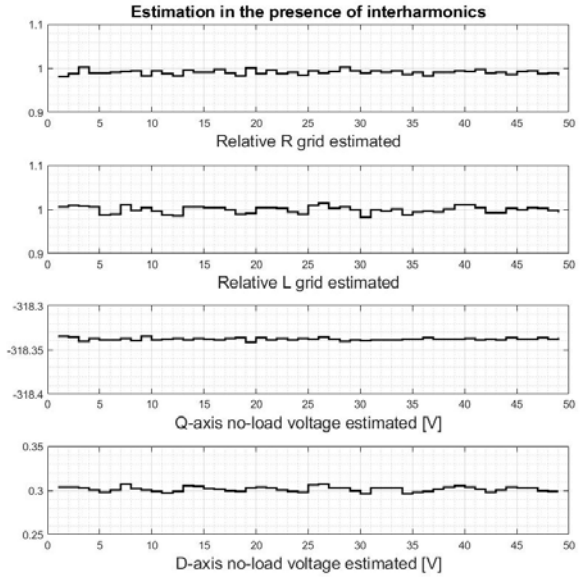


Fig. 16. The impact of interharmonics on estimates $R_g$ and $L_g$, and on estimates of no-load voltages.

## REFERENCES


[1] A. Riccobono, E. Liegmann, A. Monti, F. Castelli Dezza, J. Siegers, E. Santi, "Online wideband identification of three-phase AC power grid impedances using an existing grid-tied power electronic inverter", *17th IEEE Workshop on Control and Modeling for Power Electronics (COMPEL)*, 2016.

[2] D. Martin, E. Santi, A. Barkley, "Wide Bandwidth System Identification of AC System Impedances by Applying Perturbations to an Existing Converter", *IEEE Energy Conversion Congress and Exposition,* Sep. 2011.

[3] L. Harnefors, H.-P. Nee, "A General Algorithm for Speed and Position Estimation of AC Motors", *IEEE Tran. Industrial Electronics*, 47(1), pp. 77-83, Feb. 2000.

[4] A. V. Adebayo, C. T. Gaunt, K. O. Awodele, M. Malengret, "Online Thévenin Equivalent Impedance Measuring System", *IEEE PES/IAS PowerAfrica Conference*, pp 295-300, 2019.

[5] R. Raja, T. Sebastian, M. Wang, M.Chowdhury, "Position Estimation using PWM Excitation Method with Minimized Ripple Current", *9th International Symposium on Sensorless Control for Electrical Drives (SLED),* Helsinki, Finland, pp. 132-137, 2018.

[6] M. Jaksic, Z. Shen, I. Cvetković, D. Boroyevich, R. Burgos, C. DiMarino, and F. Chen, "Medium-Voltage Impedance Measurement Unit for Assessing the System Stability of Electric Ships", *IEEE Trans. Energy Conversion*, 32(2), June 2017, pp. 828-841.

[7] S. Neshvad, S. Chatzinotas, and J. Sachau, "Wideband Identification of Power Network Parameters Using Pseudo-Random Binary Sequences on Power Inverters", *IEEE Trans. Smart Grid,* 6(5), Sep. 2015, pp. 2293 – 2301.

[8] M. Berg, T. Messo, T. Roinila, and H. Alenius, "Impedance Measurement of Megawatt-Level Renewable Energy Inverters Using Grid-Forming and Grid-Parallel Converters", *The International Power Electronics Conference*, 2018, pp. 4205-4212.

[9] L. Hou, B. Liu, H. Shi, H. Yi, and F. Zhuo, "New Techniques for Measuring Islanded Microgrid Impedance Characteristics Based on Current Injection", *The 2014 International Power Electronics Conference,* pp. 577-581.

[10] A. Arefifar, and W. Xu, "Online Tracking of Power System Impedance Parameters and Field Experiences", *IEEE Trans. Power Delivery,* 24(4), Oct. 2009, pp. 1781-1788.

[11] A. Arancibia, C.A. Soriano-Rangel, F. Mancilla-David, R. Ortega, K. Strunz, "Finite-time Identification of the Thevenin Equivalent Parameters in Power Grids", *Electrical Power and Energy Systems,* Vol. 116, 2020, 105534 (preprint).

[12] B. Wen, D. Boroyevich, R. Burgos, P. Mattavelli, and Z. Shen, "Small-Signal Stability Analysis of Three-Phase AC Systems In the Presence of Constant Power Loads Based on Measured *d-q* Frame Impedances", *IEEE Trans. Power Electronics*, 30(10), Oct. 2015, pp. 2952-2963.

[13] X. Wang, F, Blaabjerg, and W. Wu, "Modeling and Analysis of Harmonic Stability in an AC Power-Electronics-Based Power System", *IEEE Trans. Power Electronics,* 29(12), Dec. 2014, pp. 6421-6432.

[14] S. Corsi, and G.N. Taranto, "A Real-Time Voltage Instability Identification Algorithm Based on Local Phasor Measurements", *IEEE Trans. Power Systems,* 23(3), Aug. 2008, pp. 1271-1279.

[15] S.N. Vukosavic, A.M. Stankovic, "Electronic Power Waves in Networks of Inverters", *North American Power Symposium (NAPS),* Fargo, ND, Sep. 2018.

[16] C.J. O'Rourke, M.M. Qasim, M.R. Overlin, and J.L. Kirtley, "A Geometric Interpretation of Reference Frames and Transformations: dq0, Clarke, and Park", *IEEE Trans. Energy Conversion*, 34(4), Dec. 2019, pp. 2070 – 2083.

[17] Y. Liu1, Z. Li, Y. Yang, J. Liu, "A Novel On-line Identification for Thevenin Equivalent Parameters of Power System Regarding Persistent Disturbance Condition", *2016 China International Conference on Electricity Distribution (CICED 2016)*, Xi'an, Aug. 2016, Paper No. CP0119

[18] G.H. Golub, C.F. Van Loan, *Matrix Computations (3-rd Ed.)*, Johns Hopkins U. Press, Baltimore, 1996.

[19] S. Boyd, L. Vandenberghe, *Introduction to Applied Linear Algebra,* Cambridge U. Press, 2018.

[20] Texas Instruments, *C2000 Key Technology Guide*, Application Report, August 2019, Available: http://www.ti.com/lit/an/spracn0/spracn0.pdf (last accessed 2Feb2020).

[21] S.N. Vukosavic, *Grid Side Converters -Design and Control*, Springer, 2018.

[22] W.H. Press, B.P. Flannery, S.A. Teukolsky, W.T. Vetterling, *Numerical Recipes in C*, Cambridge U. Press, 1992.

[23] *DM2020 Data manual*, MOOG Italiana S.r.l., Casella, Italy, 2011, https://www.moog.com/content/dam/moog/literature/ICD/DM2020%20Manual%20eng%20web.pdf


**Slobodan N. Vukosavic** (M'93, SM'12) was born in Sarajevo, Yugoslavia, in 1962. He received the B.S., M.S., and Ph.D. degrees from the University of Belgrade, Belgrade, Yugoslavia, in 1985, 1987, and 1989, respectively, all in Electrical Engineering. He was with the Nikola Tesla Institute, Belgrade, Yugoslavia, until 1988, when he joined the ESCD Laboratory of Emerson Electric, St. Louis, MO. Since 1991, he worked with Vickers Electric Company and MOOG Electric. S.N. Vukosavic is with the Department of Electrical Engineering, The University of Belgrade, and Serbian Academy of Sciences and Arts. His interests include digital control, power conversion in renewable energy sources, and power quality. He has published over 100 papers, 4 textbooks and 7 monographs, and has completed over 40 large R/D and industrial projects.

**Aleksandar M. Stanković** (F'05) received the Ph.D. degree in electrical engineering from the Massachusetts Institute of Technology, Cambridge, MA, USA, in 1993. From 1993 to 2010, he was with Northeastern University, Boston. He currently serves as an A.H. Howell Professor at Tufts University, Medford, MA, USA. He has held visiting positions at the United Technologies Research Center (sabbaticals in 2000 and 2007) and at L'Universite de Paris-Sud and Supelec (in 2004). He is a coeditor of a book series on power electronics and power systems for Springer. Since 1996, Dr. Stanković has served an Associate Editor of the IEEE TRANSACTIONS ON POWER SYSTEMS, IEEE TRANSACTIONS ON SMART GRID, and IEEE TRANSACTIONS ON CONTROL SYSTEMS TECHNOLOGY for over 20 years.